

Nuclear shell effects in helion polarization phenomena

J. S. Hanspal,* R. J. Griffiths, and N. M. Clarke

Wheatstone Physics Laboratory, King's College, Strand, GB-London WC2R 2LS, United Kingdom

(Received 8 August 1984)

The helion elastic scattering cross section and polarization data for a target mass range $16 \leq A \leq 48$ are fitted using the optical model, where the spin-orbit potential is deduced microscopically. The quenching effects on the spin-orbit potential of the nucleons occupying the spin-unsaturated shells in the target have been included through the nucleon-nucleus interaction in two different ways, one being an *ad hoc* approach, while the other is based on more rigorous calculations recently presented in the literature. Both methods produce very similar results and the predictions are comparable to the completely phenomenological approach, despite the contrasting shapes of the microscopic and phenomenological spin-orbit potentials. The valence quenching effects on elastic polarization are found to be small. The deduced N-nucleus spin-orbit potential strengths are consistent with the values obtained using realistic nucleon-nucleon calculations for the targets near closed-shell nuclei. The effects of using different nuclear densities and the sensitivity to the helion wave function are described.

I. INTRODUCTION

The origin of the nucleon-nucleus (N- \mathcal{N}) spin-orbit (SO) interaction has been the subject of intensive study for over thirty years. Unlike the case of an electron moving in a Coulomb field, where the force arises from electromagnetic considerations, the difficulties in the nuclear case arise from the complex meson exchange nature of the nucleon-nucleon (N-N) interaction. In spite of the difficulties, some notable contributions to its understanding have been made,¹⁻⁷ and, recently, some new aspects of the underlying dynamics have come to light.⁸⁻¹³

It has become particularly relevant to inquire about the nature of this force with the availability of polarization measurements involving complex projectiles such as deuterons, tritons, helions, and ^{6,7}Li. The folding model provides a link between the polarization measurements and the N-N interaction. It is necessary in such an approach to consider the internal structure of both the projectile and the target nuclei. In either particle a cluster approach can be used to separate the spin-saturated (core) nucleons (SS) from the spin-unsaturated (valence) nucleons (SUS).

Spin-1 projectiles can be assumed to consist of a deuteron cluster moving around the $(A-2)$ core,¹⁴ with the SO interaction arising from the deuteron averaged over the relative motion wave function between the clusters. Similarly, ⁷Li can be considered as a n-⁶Li or α -t cluster. However, for the lithium particles, these prescriptions are not successful in explaining the vector analyzing powers and it is necessary to include the effects of projectile excitation.¹⁵ For incident particles such as ¹³C, Moffa¹⁶ considers the SO force to arise solely from the valence nucleon (in the $p_{1/2}$ shell model orbital) and the resultant potential is obtained by convoluting the nucleon-nucleus (N- \mathcal{N}) interaction with the nucleon wave function and the target density. This approach produces a shell-dependent potential; it being attractive (repulsive) for the valence nu-

cleon occupying a $j=l+\frac{1}{2}(l-\frac{1}{2})$ state.

The effect of valence nucleons outside the spin-saturated core should be included for the target as well as the projectile. This is particularly important for the following analysis of 33 MeV helions scattering from light nuclei in which the nucleons in the spin unsaturated shells are an appreciable fraction of the total (e.g., ⁴⁸Ca). The microscopic SO potential was deduced by an extension of the method of Watanabe¹⁷ by Keaton *et al.*¹⁸ The N- \mathcal{N} interaction incorporates the valence quenching effects described by Scheerbaum.¹² Apart from consistency with Scheerbaum's work, the cancellation of the spin-saturated core contribution by the inclusion of the valence effects provides a possible mechanism for the anomalously small diffuseness ($a_s \simeq 0.2$ fm) characteristic observed in the phenomenological helion SO potential.¹⁹⁻²⁴ Also, the microscopic description is expected to lead to a unique helion SO potential, in contrast to the ambiguities observed in phenomenological analyses.^{23,25}

The paper is organized so that in Sec. II a brief description of the spin-orbit folding model is given, followed in Sec. III by the form of the helion wave function used. Sec. IV describes how the spin-saturated core and spin-unsaturated valence parts of the N- \mathcal{N} SO potentials were constructed. In Sec. V the ³He- \mathcal{N} SO potentials are expressed in terms of these N- \mathcal{N} SO potentials. Section VI illustrates the methods used to calculate the target densities on which the folding potentials depend. This is followed in Sec. VII by the data predictions, and in Sec. VIII the deduced strengths of the N- \mathcal{N} SO potentials are compared with those arrived at from the N-N effective interactions. Finally, in Sec. IX the conclusions are presented.

II. THE FOLDING MODEL

The simple approach of Keaton *et al.*¹⁸ was adopted in calculating the ³He- \mathcal{N} SO potential. The method is similar to those given by Abul-Magd and El-Nadi²⁶ and

Samaddar *et al.*²⁷

Provided the distortion and dissociation term in the total wave function for the helion-nucleus system is ignored and the internal helion wave function $\chi(\rho, \mathbf{r})$ is assumed to be spherically symmetric, then for a N- \mathcal{N} SO interaction

$$v_s^N(r) = V_s^N \frac{1}{s} \frac{dg(s)}{ds} \sigma \cdot \mathbf{1}, \quad (2.1)$$

the ${}^3\text{He}$ - \mathcal{N} SO potential becomes¹⁸

$$U_s^h(R) = V_s^h \frac{1}{R} \frac{dG(R)}{dR} \sigma \cdot \mathbf{L}, \quad (2.2)$$

where

$$V_s^h = \frac{1}{3} V_s^N, \quad (2.3)$$

and

$$G(R) = \int d\rho d\mathbf{r} |\chi(\rho, r)|^2 g(s). \quad (2.4)$$

The coordinate system is shown in Fig. 1. V_s^N and $g(s)$ are the strength (or depth) parameter and form factor of the N- \mathcal{N} SO potential, respectively. σ^N (σ) and $\mathbf{1}$ (\mathbf{L}) correspond, respectively, to the spin of the nucleon (helion) and its orbital angular momentum about the target. It will be noted that the strength of the potential for the helion, V_s^h , is expected to be one-third of that for the nucleon.¹⁶

III. THE HELION WAVE FUNCTION

For a Gaussian projectile wave function it can be shown²⁷ that the six-dimensional integral (2.4) reduces to a one-dimensional integral. Because of the simplicity this introduces in the numerical evaluation of the potential, for the helion it was taken to be

$$\chi(\rho, r) = N \exp[-\gamma(2\rho^2 + \frac{3}{2}r^2)], \quad (3.1)$$

with

$$N = \left(\frac{2\sqrt{3}\gamma}{\pi} \right)^{3/2}. \quad (3.2)$$

The value of γ was fixed to 0.0686 fm^{-2} , which is satisfactory in reproducing the electromagnetic form factor for the helion.²⁸

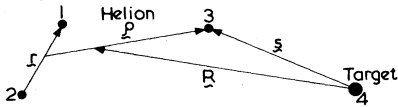


FIG. 1. The coordinate system used in the derivation of the helion potential. \mathbf{R} joins the center of mass (c.m.) of the projectile with the c.m. of the target, and ρ joins the c.m. of nucleons 1 and 2 to nucleon 3.

IV. THE N- \mathcal{N} SO POTENTIAL

A systematic and thorough investigation of the N- \mathcal{N} SO potential in terms of the N-N interaction by Scheerbaum,¹⁰⁻¹² within the Bruecker-Hartree-Fock approximation,²⁹ has led to some interesting results. According to these calculations, a nucleon interacting with the spin-saturated core of a nucleus produces a SO splitting so that (as usual) the $j=l+\frac{1}{2}$ energy level is placed below the $j=l-\frac{1}{2}$ level.^{10,11} But, surprisingly, its interaction with nucleons in the spin-unsaturated shells tends to invert the positioning of these doublet levels.¹² This produces a quenching of the SO potential. The total potential may therefore be split into two components:

$$v_s^N(r) = v_{SS}(r) + v_{SUS}(r). \quad (4.1)$$

A. SS core contribution

In calculations including the exchange effects, the contribution to the SS core component arises in two parts: in the first order due to the effective N-N SO interaction,¹⁰ and in the second order due to the tensor component¹¹ of this interaction. For nuclei with an $N=Z$ SS core (which is so for the targets considered here), the potential is expressed¹¹ as

$$v_{SS}(r) = \left[-\frac{\pi}{2} S^{30} + K_T^a \rho_c(r) \right] \frac{1}{r} \frac{d\rho_c}{dr} \sigma \cdot \mathbf{1}, \quad (4.2)$$

where

$$S^{30} = \frac{3}{q} \int_0^\infty s^3 j_1(gs) g^{30}(s) ds \quad (4.3)$$

is the strength of the first order contribution and K_T^a is the parametrized two-body tensor interaction strength (see Ref. 11). ρ_c is the core density of the nucleus, q ($=0.7 \text{ fm}^{-1}$) is the average "wavelength" of the density distribution at the nuclear surface, j_1 is the first order spherical Bessel function, and g^{30} is the triplet-odd (30) effective N-N SO interaction.

Although the second order tensor contribution was required in the bound state calculations to correctly predict the splittings for the normally occupied levels,¹¹ a parallel derivation to Scheerbaum's by Brieva and Rook (BR) (Ref. 7) for the N- \mathcal{N} scattering was shown to be sufficient to first order. This is consistent with Scheerbaum's earlier findings¹⁰ that Eq. (4.2) to first order correctly predicts the splittings of the valence (normally unoccupied) levels. The N- \mathcal{N} SO potential of Brieva and Rook was

$$v_{SS}(r) = K_{BR} \frac{1}{r} \frac{d\rho_c}{dr} \sigma \cdot \mathbf{1}, \quad (4.4)$$

with

$$K_{BR} = \frac{\pi}{3} [B^D(\rho, E) - R^E(k; \rho, E)], \quad (4.5)$$

where B^D and R^E represent the strengths of the direct and exchange contributions, and k corresponds to the local momentum. For low energy ($k \rightarrow 0$) projectiles, the strength K_{BR} reduces to

$$K_{\text{BR}} = \frac{\pi}{2} B^{30}, \quad (4.6)$$

where

$$B^{30} = \int_0^\infty t^{30}(s) s^4 ds \quad (4.7)$$

and t^{30} is the triplet-odd effective N-N SO interaction, which for the scattering case could be complex⁷ in contrast to g^{30} .

Invoking Eq. (4.7) it will be seen that Eqs. (4.2) and (4.4) are equivalent to first order (for $qs \ll 1$), and the values of S^{30} and B^{30} are found to be in agreement for realistic N-N interactions.⁷ This formulation for the SS core component of the N- \mathcal{N} SO interaction has been used in the following.

B. SUS valence shell contribution

The quenching of the SO splitting by the SUS valence nucleons has been derived explicitly by Scheerbaum¹² to first order in the Brueckner-Hartree-Fock expansion. Its source is the exchange term in the interaction energy equation and its repulsive characteristic comes from the negative sign of this term. The predominant N-N interactions participating are found to be the central and the tensor components. The method¹² has been successfully applied by Goodman and Boryscowicz³⁰ to explain the mass dependence of the $l=5$ proton SO splitting.

Because of the nonlocal characteristic of the SUS effect,¹² an *ad hoc* local potential—of the derivative valence density form with its sign reversed—was constructed as done by Cohler *et al.*³¹ The contribution may be expressed as

$$v_{\text{SUS}}(r) = -K_{\text{BR}} \frac{\beta}{r} \frac{d\rho_v}{dr} \sigma \cdot \mathbf{1}, \quad (4.8)$$

where β is the relative strength of the valence and core parts, ρ_v is the density of the valence nucleons in the SUS shells, and K_{BR} is given by Eq. (4.5). This has been included in the prediction³¹ of the 50 MeV $^{24}\text{Mg}(\bar{p}, p)^{24}\text{Mg}$ data of Lewis *et al.*³² and comparison with the conventional Blin-Stoyle prescription indicated detectable differences due to the SUS effects. Furthermore (and this was not explicitly mentioned by Cohler *et al.*), comparison of the SO potentials for the two cases revealed that the inclusion of SUS quenching reduced the “radius parameter” of the potential (see Fig. 1 of Ref. 31). Therefore, SUS effects provide an alternative mechanism to those discussed in the literature^{3,4} for this reduction when compared to the real central potential. Also, Dudek *et al.*³³ have recently used this approach to correctly predict the characteristic oscillatory behavior of the SO radius and strength parameters for the deformed nuclei as a function of the nuclear mass.

The work of Scheerbaum has recently been extended by Love¹³ to include the effects of the SUS valence nucleons in the N- \mathcal{N} scattering. Within certain approximations, a local SO contribution of the form

$$v_{\text{SUS}}(r) = \frac{J(k^2)}{24\pi} \sum_{nl} [lN_{>} - (l-1)N_{<}] \frac{u_{nl}^2(r)}{r^2} \sigma \cdot \mathbf{1} \quad (4.9)$$

was obtained for spherical targets. Here, $J(k^2)$ is the strength of the valence contribution arising from the central (t_C) and tensor (t_T) N- \mathcal{N} interaction components, and is given by

$$J(k^2) = 4\pi \int_0^\infty ds s^4 [t_C(s) - t_T(s)] \frac{3j_l(ks)}{ks}. \quad (4.10)$$

nlj correspond to the valence level quantum numbers; $N_{>}$ and $N_{<}$ are the respective occupation probabilities of the $j=l+\frac{1}{2}$ and $j=l-\frac{1}{2}$ levels; and u_{nl} is the complete radial part of the single particle orbital.

Comparing Eqs. (4.8) and (4.9), it is interesting to note the differences in the analytical forms between the two approaches. Therefore if the predictions are sensitive to the SUS quenching effects, this should be clearly reflected in the fits to the data.

C. Relative strengths of the SS and SUS contributions

Combining the results of Secs. IV A and IV B, the N- \mathcal{N} SO potential for the *ad hoc* approach becomes

$$v_s^{\text{N}}(r) = K_{\text{BR}} \left[\frac{1}{r} \frac{d\rho_c}{dr} - \frac{\beta}{r} \frac{d\rho_v}{dr} \right] \sigma \cdot \mathbf{1}, \quad (4.11)$$

and using the standard expressions for the density distributions for the more rigorous approach of Love,¹³ it may be expressed as³⁴

$$v_s^{\text{N}}(r) = K_{\text{BR}} \left[\frac{1}{r} \frac{d\rho_c}{dr} + \nu \sum_{nl} \alpha_{nl} \frac{\rho_{nl}}{r^2} \right] \sigma \cdot \mathbf{1}, \quad (4.12)$$

where ν is the relative strength of the valence to core contribution, ρ_{nl} is the density of the valence level nl , and

$$\alpha_{nl} = \left[\frac{lN_{>} - (l+1)N_{<}}{N_{>} + N_{<}} \right]. \quad (4.13)$$

Utilizing Eq. (4.6), the factor ν may be approximated by

$$\nu = \frac{J(k^2)}{3\pi B^{30}}, \quad (4.14)$$

and, assuming $B^{30} \approx 36 \text{ MeV fm}^5$ (Ref. 7), coupled with the results of Love,¹³ its values for some targets are listed in Table I. ν lies in the range 1.2–1.5. Of course, there are uncertainties in its value as a result of errors in $J(k^2)$ and B^{30} . For example, $B^{30} \approx 47 \text{ MeV fm}^5$ is derived from the Yale or Gammel-Thaler effective N-N interactions, in

TABLE I. The strength of the N- \mathcal{N} SO potential due to SUS shells (Ref. 13) and its comparison to the contribution from the SS core. The projectile energy E is measured in MeV and $J(k^2)$ is in MeV fm⁵.

Target	Energy (E)	$J(k^2)$	t_T/t_C	ν
¹² C	45.5	396	2.8	1.2
²⁸ Si	30	486	3.0	1.4
²⁸ Si	135	130	1.5	0.4
⁴⁸ Ca	15	509	14	1.5
⁴⁸ Ca	30	459	14	1.4

which case ν becomes confined to the range 0.9–1.1. The value of ν decreases even more if B^{30} is derived from the free N-N interactions. In view of the uncertainties in ν around a value of unity and (as will be illustrated in Sec. VII) the relative insensitivity of the angular distributions to its exact value in this vicinity, ν was fixed at 1.0.

As for ν , the weight (β) for the SUS contribution in Eq. (4.11) will in some way be dependent on B^{30} , $J(k^2)$, and the valence orbitals. However, it is not clear what the exact relation should be. Cohler *et al.*³¹ were able to get reasonable reproduction of some extensive $^{24}\text{Mg}(\bar{p}, p)^{24}\text{Mg}$ data³² taken at 50 MeV using $\beta=1.0$. On the other hand, Dudek *et al.*³³ required its value to be ≈ 0.25 for protons and ≈ 0.4 for neutrons to correctly predict the radius and strength of the SO potential for deformed nuclei. However, they³³ restricted their analysis to the mass range $A \geq 100$ and an extrapolation to the presently considered mass range may not necessarily be valid. This is especially so in light of the comment by Dudek *et al.*³³ that for the deformed nuclei considered by them, the single-particle orbital momentum is not a well-defined quantity and, consequently, the notion of spin saturation loses its meaning in the sense defined by Scheerbaum.¹⁰ Bearing in mind the completely *ad hoc* nature of including the SUS effect, and to maintain consistency with the work of Cohler *et al.*,³¹ β was fixed to 1.0. With this assumption the dependence of SUS component in going from one nucleus to another comes entirely from the valence density. The effect of reducing β will be discussed in Sec. VIII.

V. ^3He -NUCLEUS SO POTENTIAL

In the following, the helion SO potential calculated using Eqs. (4.11) and (4.12) for the N- \mathcal{N} SO interaction will be referred to as the *ad hoc* model and present model, respectively. For the former, due to the derivative density form of Eq. (4.11), the form factor $G(R)$ simply becomes

$$G(R) = \int d\rho d\mathbf{r} |x(\rho, r)|^2 [\rho_c(s) - \beta\rho_v(s)]. \quad (5.1)$$

In other words, the difference between the SS core and SUS valence densities is averaged over the helion wave function.

For the present model, however, the valence contribution is not of the derivative form. Therefore to evaluate the helion form factor, a function $g_{nl}(s)$ for the valence part, defined by

$$\frac{1}{s} \frac{dg_{nl}(s)}{ds} \equiv \frac{\rho_{nl}}{s^2}, \quad (5.2)$$

was numerically calculated. Since ρ_{nl} satisfies the boundary conditions

$$\lim_{s \rightarrow 0} \frac{\rho_{nl}}{s} = 0 \quad (5.3)$$

and

$$\lim_{s \rightarrow \infty} \frac{\rho_{nl}}{s} = 0, \quad (5.4)$$

g_{nl} was computed using

$$g_{nl}(s) = \int_0^s \frac{\rho_{nl}(x)}{x} dx. \quad (5.5)$$

The form factor may now be expressed as

$$G(R) = \int d\rho d\mathbf{r} |\chi(\rho, r)|^2 [\rho_c(s) + \nu \sum_{nl} \alpha_{nl} g_{nl}(s)]. \quad (5.6)$$

For both models, the strength of the helion SO potential, from Eq. (2.3), is

$$V_s^h = \frac{1}{3} K_{BR},$$

or, if Eq. (4.6) is assumed,

$$V_s^h = \frac{\pi}{6} B^{30}. \quad (5.7)$$

So utilizing a realistic N-N effective interaction to calculate B^{30} , in principle, fixes V_s^h , and since the geometry of the potential is determined by the helion wave function and the core and valence densities, there are no free parameters. However it has been pointed out¹⁰ that the value of B^{30} (or S^{30}) depends on the type of N-N interaction used. Consequently, V_s^h was allowed to be a free parameter to obtain the best fit to the data and the deduced values of B^{30} were compared with the values derived from some popular N-N interactions.

VI. TARGET DENSITY

The simple independent particle shell model approach of Batty and Greenlees (BG) (Ref. 35) was utilized for calculating the target densities. The nucleons moved in Saxon-Woods potentials of “standard geometry,”³⁵ listed in Table II, and the depths of the central (V_0) and spin-orbit (V_{SO}) potentials were adjusted to produce the binding energies of the last proton and neutron. The densities of the SS core and SUS valence shells were then computed in accordance with

$$\rho_c(r) = \sum_{nlj}^{\text{core}} \frac{(2j+1)}{4\pi} |u_{nlj}(r)|^2 \quad (6.1)$$

and

$$\rho_v(r) = \sum_{nlj}^{\text{valence}} \frac{N_v(nlj)}{4\pi} |u_{nlj}(r)|^2, \quad (6.2)$$

TABLE II. The “standard geometry” parameters used for the shell model potential to evaluate matter densities. All lengths are measured in fm.

Nucleon	r_0	a_0	r_s	a_s	r_c	Reference
Proton	1.28	0.76	1.09	0.60	1.2	35
Neutron	1.19	0.75	1.19	0.75		36

TABLE III. The optical model parameters used in comparing the microscopic SO potential fits with phenomenology. Also listed is the deduced N_{ν} strength B^{30} .

Target	Model	V_R (MeV)	r_R (fm)	a_R (fm)	W_V (MeV)	W_D (MeV)	r_I (fm)	a_I (fm)	V_S (MeV)	r_S (fm)	a_S (fm)	$\frac{\chi^2}{N}$	$\frac{\chi^2}{N}$	J_R (MeV fm ³)	B^{30} (MeV fm ⁵)
¹⁶ O	Present or <i>ad hoc</i>	121.0	1.07	0.805	0.0	8.44	1.55	0.830				29.0	32.2	404	31.2
¹⁶ O	Present or <i>ad hoc</i>	121.0	1.07	0.805	0.0	8.44	1.55	0.830				29.1	32.3	404	31.8
¹⁶ O	Phenomenology	122.8	1.07	0.800	0.0	8.35	1.55	0.850	1.49	1.07	0.300	30.1	52.6	403	36.9
¹⁷ O	Present	123.8	1.07	0.807	0.0	9.54	1.49	0.830				27.3	17.2	405	36.0
¹⁷ O	<i>ad hoc</i>	123.8	1.07	0.808	0.0	9.55	1.48	0.830				27.0	16.8	405	36.0
¹⁷ O	Phenomenology	122.9	1.07	0.810	0.0	9.65	1.51	0.840	2.20	1.10	0.210	17.8	13.4	404	49.8
¹⁸ O	Present	120.0	1.07	0.800	0.0	14.11	1.32	0.830				11.1	22.4	382	46.1
¹⁸ O	<i>ad hoc</i>	120.0	1.07	0.800	0.0	14.11	1.32	0.830				10.4	21.9	382	46.1
¹⁸ O	Phenomenology	121.0	1.07	0.790	0.0	13.80	1.35	0.830	2.16	1.08	0.230	5.9	5.1	380	
²⁴ Mg	Present	191.2	1.00	0.743	18.39	0.0	1.64	0.950				65.3	39.2	450	98.3
²⁴ Mg	<i>ad hoc</i>	190.5	1.00	0.746	18.64	0.0	1.63	0.960				64.4	27.0	450	71.4
²⁴ Mg	Phenomenology	191.6	1.00	0.744	18.27	0.0	1.68	0.944	3.82	1.05	0.278			450	
²⁶ Mg	Present	164.3	1.12	0.673	29.95	0.0	1.40	0.961				133.5	15.8	455	354.0
²⁶ Mg	<i>ad hoc</i>	173.4	1.12	0.677	35.09	0.0	1.33	0.967				150.9	14.7	477	113.7
²⁶ Mg	Phenomenology	160.2	1.12	0.677	31.66	0.0	1.37	0.949	7.19	0.96	0.251			477	
³² S	Present	146.4	1.07	0.798	18.04	0.0	1.64	0.911				10.0	5.9	391	106.0
³² S	<i>ad hoc</i>	146.4	1.07	0.799	18.04	0.0	1.64	0.912				10.3	4.2	392	64.9
³² S	Phenomenology	146.2	1.07	0.822	18.33	0.0	1.63	0.938	3.25	1.08	0.250			392	
⁴⁰ Ca	Present or <i>ad hoc</i>	171.2	0.92	0.906	9.67	0.0	1.90	0.717				3.98	39.0	348	55.5
⁴⁰ Ca	Present or <i>ad hoc</i>	171.2	0.92	0.906	9.67	0.0	1.90	0.717				3.95	35.8	348	51.7
⁴⁰ Ca	Phenomenology	171.2	0.92	0.906	9.67	0.0	1.90	0.717	2.97	1.04	0.260	4.16	16.7	348	
⁴⁴ Ca	Present	172.6	0.90	0.906	12.03	0.0	1.32	0.774				2.32	3.9	326	62.0
⁴⁴ Ca	<i>ad hoc</i>	172.6	0.90	0.906	12.03	0.0	1.32	0.774				2.27	3.4	326	55.7
⁴⁴ Ca	Phenomenology	172.6	0.90	0.906	12.03	0.0	1.32	0.774	3.54	1.00	0.340	2.00	1.8	326	
⁴⁸ Ca	Present	156.5	0.99	0.815	12.07	0.0	1.75	0.776				2.97	17.6	325	71.0
⁴⁸ Ca	Present	156.5	0.99	0.815	12.07	0.0	1.75	0.776				2.58	16.3	325	66.4
⁴⁸ Ca	<i>ad hoc</i>	156.5	0.99	0.815	12.07	0.0	1.75	0.776				2.87	16.7	325	50.3
⁴⁸ Ca	<i>ad hoc</i>	156.5	0.99	0.815	12.07	0.0	1.75	0.776				2.65	19.4	325	46.2
⁴⁸ Ca	Phenomenology	156.5	0.99	0.815	12.07	0.0	1.75	0.776	3.16	0.95	0.188	2.92	8.2	325	

where N_v is the occupation number of the valence shell nlj and u_{nlj} is the complete radial wave function.

For targets with $16 < A \leq 26$ the SS core was ^{16}O , and for $A > 40$ it was ^{40}Ca . For ^{32}S the core density was taken to be the sum of ^{16}O and the nucleons in the $2s_{1/2}$ level, and the valence density was due to nucleons in the $1d_{5/2}$ level.

To test the sensitivity of the helion polarization distributions to the target densities, the semi-self-consistent densities of Brown, Massen, and Hodgson (BMH) (Ref. 37) were also used in evaluating the SO potentials for ^{16}O and ^{40}Ca . The densities were provided by Brown.³⁸ Aside from these two targets, only the BG (Ref. 35) densities were used.

VII. DATA PREDICTION

The folding model SO potentials were calculated in steps of 0.1 fm within the range $0.1 \leq r \leq 14.6$ fm from the target center, and the computer program RAROMP (Ref. 39) was used to simultaneously fit the cross section and polarization distributions. The closed or near-closed shell target data considered were ^{16}O (Ref. 24), $^{17,18}\text{O}$ (Ref. 40), and $^{40,44,48}\text{Ca}$ (Ref. 25), and those in the mid-mass range were ^{24}Mg (Ref. 41), ^{26}Mg (Ref. 21), and ^{32}S (Ref. 23). The central potentials were phenomenological and their parameters were kept fixed to the values derived in the relevant references^{40,25,41,21,23} which are listed in Table III. Where possible, the central potentials were chosen to be "physically meaningful" in the sense described by Trost *et al.*⁴²

A. The ^{48}Ca target

Since the present model is, strictly, only applicable for spherical nuclei with SUS shells, the effect of the valence nucleons satisfying this criterion is expected to be largest for the ^{48}Ca target. Hence this target will be considered first.

The contributions to the data from the SS core and SUS valence parts of the SO potential are depicted in Fig. 2. This was done by achieving the best fit with the total SO potential and then switching off the valence part to get the fit due to the core contribution and vice versa. The fit to the polarizations with the full potential is shown in Fig. 4, where it is compared to the predictions of the *ad hoc* and phenomenological models. The polarization predictions due to the core and valence parts (Fig. 2) are in anti-phase over the whole angular range, as expected from the opposite sign of the potentials. The important feature is that the core contribution alone, when normalized, is sufficient to account for the data. This aspect is again reflected for the *ad hoc* model (Fig. 4), since the predictions due to the two folding models are almost indistinguishable. So the valence effects are difficult to extract even for this extreme case.

The underlying reason for this insensitivity is illustrated in Fig. 3, which depicts the core and valence contributions to the SO potential for both folding models. The valence effects are suppressed due to the much shorter range of the valence potential compared to the core contribution and over the most important surface region the differ-

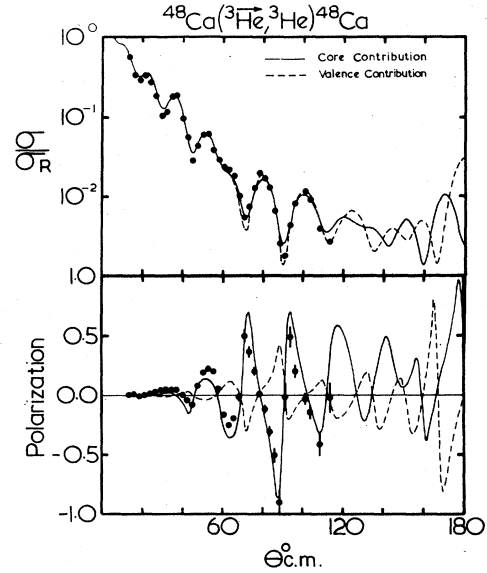


FIG. 2. Comparison of the predictions due to the core and valence components of the SO potential for the present model.

ences are essentially those of scale rather than shape. Also as a consequence of the shorter range of the valence component, it is clear that the angular distribution is insensitive to the exact value of the relative strength v within the allowable range. A similar argument applies for β .

Also, for ^{48}Ca , the sensitivity of the data to the helion wave function was investigated. The fits due to the *ad hoc* and present models with a Gaussian ^3He wave function [Eq. (3.1)] were compared with those where it was replaced with a delta function:

$$|\chi(\rho, r)|^2 = \delta(\rho)\delta(r). \quad (7.1)$$

Although this produced a narrowing effect on the potentials, as far as the polarization was concerned, no difference was found. The χ^2 contributions to the cross section and polarization distributions are compared in Table III.

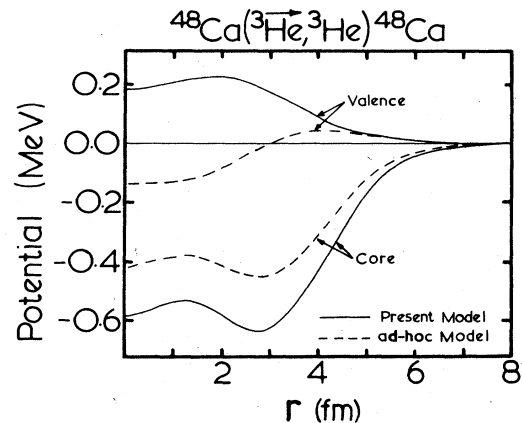


FIG. 3. The core and valence parts of the SO potentials for the present and *ad hoc* models. The nuclear surface as defined by $r_1 A^{1/3}$ is at $r = 6.4$ fm.

B. All targets

The folding model calculations for all the targets considered are compared with phenomenology in Fig. 4. The fits to the cross sections are not shown due to their relatively reduced sensitivity to the SO potential. There are significant differences between the two approaches (phenomenology and microscopy) for the oxygen isotopes, but these become smaller for the other targets. The microscopic fits are generally slightly inferior to the phenomenological fits but of course the microscopic approach is physically more meaningful and has few parameters. The *ad hoc* and present model predictions are almost identical. Any difference in ^{26}Mg is not confidently considered meaningful due to the large error bars assigned to the polarization data, in which case it could not be certain if the χ^2 minimization routine in RAROMP reached a meaningful minimum.

For ^{16}O and ^{40}Ca , the microscopic calculations were carried out for the BG (Ref. 35) and BMH (Ref. 37) target densities, but the two predictions in Fig. 4 are coincident over the full angular range. Therefore it is sufficient to use the simple independent particle shell model densities for generating the folding model SO potentials in helion scattering.

Figure 5 compares the microscopic and phenomenological SO potentials for all the targets. The contrast between

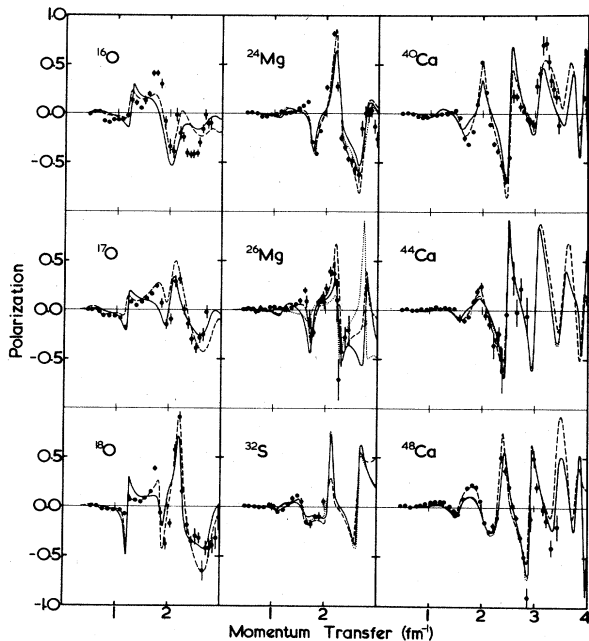


FIG. 4. Polarization predictions using the microscopic and phenomenological SO potentials. For ^{16}O and ^{40}Ca the solid lines are fits due to the folding potential generated using the BMH densities and the dotted curves using BG densities. For all other targets the solid and dotted curves represent fits due to the present and *ad hoc* models, respectively. The dashed curves are due to complete phenomenology in all cases. Where dotted curves are not visible, they are coincident with solid curves.

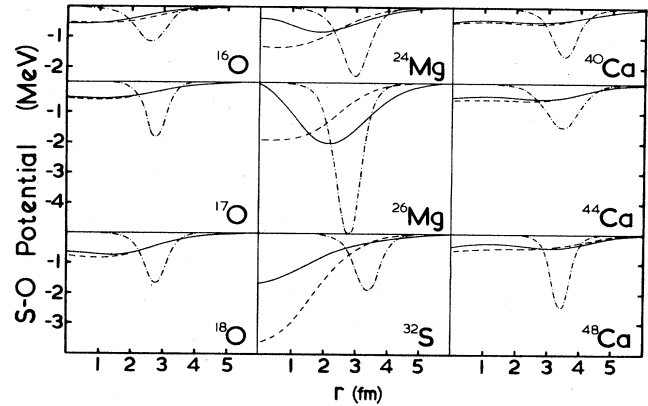


FIG. 5. Comparison of the microscopic and phenomenological SO potentials for all the targets considered. For ^{16}O and ^{40}Ca , the solid lines are due to the folding potential generated using the BMH densities and the dashed curves using BG densities. For all other targets, the solid and dashed curves correspond to present and *ad hoc* models, respectively. The chain curves are due to complete phenomenology.

the two approaches is quite striking, with phenomenological potentials (with the anomalous diffuseness parameter²⁵) being localized in the nuclear surface, whereas the microscopic potentials have appreciable magnitudes within the nucleus and generally have longer tails. Yet the fits are comparable between the two methods. Therefore the polarization data are not very sensitive to the SO potential shape, which is consistent with previous phenomenological analysis of the calcium data²⁵ where this potential was found to be ambiguous. The differences between the *ad hoc* and present model potentials near the nuclear surface are small, except for ^{26}Mg for reasons discussed earlier.

VIII. THE DEDUCED N-N SO STRENGTH B^{30}

It was pointed out in Sec. V that the strength of the helion SO potential can be expected to be consistent with the N-N effective SO interaction. The deduced values of B^{30} [see Eq. (5.7)] are listed in Table III and their variation with the target mass number is depicted in Fig. 6. Also shown in Fig. 6 for comparison are the values derived by Scheerbaum¹⁰ for the N-N SO interaction. These are illustrated as lines parallel to the A axis, with magnitudes depending on the type of N-N effective interaction used.

It will be noted that there is qualitative agreement for the oxygen and calcium isotopes. The preferred value of B^{30} (referred to as S^{30} by Scheerbaum) is, on the average, that derived from the Yale or Gammel-Thaler (see Ref. 10) effective interactions, which is somewhat higher than the $\approx 36 \text{ MeV fm}^5$ evaluated from other modern interactions.

For the intermediate targets, B^{30} is consistently higher than the theory, and the disagreement is particularly large for the present model. It must be remembered that this model assumes the targets to be spherical. Adopting the

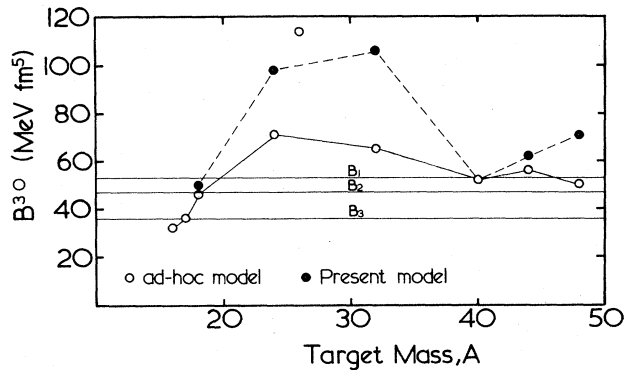


FIG. 6. The $N\text{-}N$ SO strength B^{30} derived from the helion-nucleus elastic scattering polarization. $B_1 \approx 53$ MeV fm⁵ is derived from the free Hamada-Johnston or Gammel-Thaler $N\text{-}N$ SO interactions. $B_2 \approx 47$ MeV fm⁵ is derived from the Yale or Gammel-Thaler effective $N\text{-}N$ interactions. $B_3 \approx 36$ MeV fm⁵ used the Reid soft core, Reid hard core, or Hamada-Johnston effective $N\text{-}N$ interactions.

“incorrect” form for the quenching of the core contribution may require a larger depth of the SO potential to reproduce the data and hence lead to an overestimation of B^{30} .

Despite the insensitivity of the polarization distribution to the precise values of ν , it is evident that a change in its value will affect the B^{30} value deduced. If ν is increased, the SS core contribution must be increased to restore the original magnitude of the SO potential in the surface. Consequently the overall strength of the SO potential, and hence B^{30} , must increase. For ^{48}Ca , a change in ν from 1.0 to 1.5 results in an increase in B^{30} of about 10–13% (within the constraints imposed on the surface shape). This gives an estimate of the uncertainties in B^{30} , and within these errors there is clearly an agreement between the *ad hoc* and present model approaches for nuclei near the closed-shell region. It should also be noted that an increase in ν will result in a further deviation from the theoretical B^{30} values indicated in Fig. 6. On the other hand a decrease in the value of β from unity, as suggested by Dudek *et al.*³³ will improve the agreement with the theoretical B^{30} values. Assuming that the SO interaction for the helion results essentially from the neutron, due to the protons coupling to zero spin, $\beta=0.4$ (Ref. 33) would be appropriate. As a consequence, B^{30} for ^{48}Ca would decrease by $\approx 20\%$. A decrease by this amount is certainly in order for the ^{24}Mg and ^{32}S targets to get better agreement with the theoretical SO strengths.

Another interesting possibility for the observed overestimation in Fig. 6 may be linked to the choice of the so-called “physically meaningful” real central potential family. According to Trost *et al.*⁴² this family has a target mass dependent real volume integral per particle pair, J_R , such that its value for the oxygen isotopes should be ~ 440 MeV fm³ and for the other targets considered here: ~ 330 MeV fm³. Clearly, from Table III this condition is not satisfied by the intermediate targets. Also it is known⁴³ that the depth of the SO potential is approximately proportional to the real central potential. Therefore the physical family for these targets would reduce the

SO depth, and consequently B^{30} , by roughly 25%, thus improving agreement. This is especially so for ^{24}Mg and ^{32}S for the *ad hoc* model. However the existence of this family for these two targets was not reported by Entezami *et al.*⁴¹ and Barnwell *et al.*²³ The case of ^{26}Mg will not be discussed here, as mentioned before, due to the lack of extensive and accurate data.

On the basis of the values B^{30} , the *ad hoc* model is preferred over the present model, despite the fact that both models produce very similar fits to the data. The qualitative agreement of these strengths is encouraging, because it indicates that the simple folding model approach is quite adequate in helion scattering. This also suggests that its prediction, that the helion SO potential depth is $\frac{1}{3}$ of that for the nucleon, is reasonable. This is in contrast to the conclusions of Thompson.⁴⁴

IX. CONCLUSIONS

A semimicroscopic optical model was used to predict the 33 MeV helion elastic scattering polarization and cross-section distributions from targets in the mass range $A=16\text{--}48$. The SO potential was generated using a simple folding model approach and was expressed in terms of the $N\text{-}N$ SO interaction (itself deduced from the $N\text{-}N$ interaction) and the helion wave function. The central potentials were phenomenological.

The main theme of the investigation was to find if and to what extent the helion polarizations are sensitive to the quenching effects of the valence nucleons in the SUS shell nuclei on the $N\text{-}N$ SO force. The valence effects were expressed in two different ways, leading to what were termed the *ad hoc* and (the more rigorous) present models. The SS core parts of the potentials were identical in both cases.

Both methods led to a number of interesting conclusions. Firstly, for all the targets, and particularly for those near the closed shell region, the polarization distributions were insensitive to the shape of the valence effects. This behavior was traced to be due to the much shorter range of the valence potential in comparison to the core contribution, and this consequently also explained why both approaches produced similar predictions despite differences in their analytic forms. The predictions were also insensitive to the helion wave function shape and to the methods involving a degree of sophistication in the evaluation of the target densities. The geometry of the folded SO potential was very diffuse compared to the phenomenological potential. The valence effects were unable to reproduce the sharply localized characteristic of phenomenology which is probably due to the Woods-Saxon model dependence. Even more important than the insensitivity to valence effects was the result that the polarizations were insensitive to the change in helion SO potential.

The quality of the fits using the microscopic prescriptions was comparable to phenomenology. For $^{24,26}\text{Mg}$ targets both the microscopic and phenomenological approaches were unable to fit the important forward angle regions ($q \leq 1.5$ fm⁻¹), but were both satisfactorily fitted for the larger angles.

From the depth parameters of the microscopic SO potentials the deduced $N-N$ SO potential strengths were found to be consistent with the values deduced from the $N-N$ effective SO interactions of the Yale of the Gammel-Thaler type, for targets in the closed shell region. The deduced strengths for the intermediate targets were overestimated and it was suggested that this may be related to the choice of the central potentials in addition to the uncertainties in the strength of the SUS valence component of the SO potential. The $N-N$ strengths calculated from the *ad hoc* model agree somewhat better with those obtained from calculating the shell model split-

ting energies¹⁰ than with the more rigorous present model.

In summary, the insensitivity of the helion polarization data to the SO potential is surprising, but perhaps the reaction asymmetries will be useful in isolating this force more definitively.

The authors are grateful to Dr. C. J. Batty for the use of his shell model code ANARCHY on the Rutherford Laboratory IBM 360 computer to generate the target densities, and they acknowledge financial support from the Science and Engineering Research Council during the completion of this work.

*Present address: The Florida State University, Department of Physics, Tallahassee, FL 32306.

¹J. Keelson, Phys. Rev. **82**, 759 (1951).

²R. J. Blin-Stoyle, Philos. Mag. **46**, 973 (1955).

³G. W. Greenlees, G. J. Pyle, and Y. C. Tang, Phys. Rev. Lett. **17**, 33 (1966).

⁴D. W. L. Sprung and P. C. Bhargava, Phys. Rev. **156**, 1185 (1967).

⁵D. W. L. Sprung, Nucl. Phys. **A182**, 97 (1972).

⁶G. L. Thomas, B. C. Sinha, and F. Duggan, Nucl. Phys. **A203**, 305 (1973).

⁷F. A. Brieva and J. R. Rook, Nucl. Phys. **A297**, 206 (1978).

⁸C. W. Wong, Nucl. Phys. **A104**, 417 (1967).

⁹C. W. Wong, Nucl. Phys. **A108**, 481 (1968).

¹⁰R. R. Scheerbaum, Nucl. Phys. **A257**, 77 (1976).

¹¹R. R. Scheerbaum, Phys. Lett. **61B**, 151 (1976).

¹²R. R. Scheerbaum, Phys. Lett. **63B**, 381 (1976).

¹³W. G. Love, Phys. Rev. C **20**, 1638 (1979).

¹⁴H. Amakawa and K. I. Kubo, Nucl. Phys. **A266**, 521 (1976).

¹⁵H. Nishioka, R. C. Johnson, J. A. Tostevin, and K.-I. Kubo, Phys. Rev. Lett. **48**, 1795 (1982).

¹⁶P. J. Moffa, Phys. Rev. C **16**, 1431 (1977).

¹⁷S. Watanabe, Nucl. Phys. **8**, 484 (1958).

¹⁸P. W. Keaton, Jr., E. Aufdembrink, and L. R. Veaser, Los Alamos Scientific Laboratory Report LA-4379-MS, 1970.

¹⁹W. E. Burcham, J. B. A. England, R. G. Harris, O. Karban, and S. Roman, Nucl. Phys. **A246**, 269 (1975).

²⁰O. Karban, A. K. Basak, J. B. A. England, G. C. Morrison, J. M. Nelson, S. Roman, and G. G. Shute, Nucl. Phys. **A269**, 312 (1976).

²¹M. D. Cohler, N. M. Clarke, C. J. Webb, R. J. Griffiths, S. Roman, and O. Karban, J. Phys. G **2**, L151 (1976).

²²S. Roman, A. K. Basak, J. B. A. England, O. Karban, G. C. Morrison, and J. M. Nelson, Nucl. Phys. **A284**, 365 (1977).

²³J. M. Barnwell, M. D. Cohler, N. M. Clarke, R. J. Griffiths, J. S. Hanspal, O. Karban, and S. Roman, J. Phys. G **5**, L69 (1979).

²⁴Y.-W. Lui, O. Karban, S. Roman, R. K. Bhowmik, J. M. Nelson, and E. C. Pollacco, Nucl. Phys. **A333**, 205 (1980).

²⁵J. S. Hanspal, R. J. Griffiths, N. M. Clarke, J. M. Barnwell,

O. Karban, and S. Roman, Nucl. Phys. **A427**, 297 (1984).

²⁶A. Y. Abul-Magd and M. El-Nadi, Prog. Theor. Phys. **35**, 798 (1966).

²⁷S. K. Samaddar, R. K. Satpathy, and S. Mukherjee, Nucl. Phys. **A150**, 655 (1970).

²⁸L. I. Schiff, Phys. Rev. **133**, B802 (1964).

²⁹B. H. Brandow, Rev. Mod. Phys. **39**, 771 (1967).

³⁰A. L. Goodman and J. Boryscowicz, Nucl. Phys. **A295**, 333 (1978).

³¹M. D. Cohler, R. J. Griffiths, N. M. Clarke, and J. S. Hanspal, J. Phys. G **5**, L43 (1979).

³²V. E. Lewis, E. J. Burge, A. A. Rush, D. A. Smith, and N. K. Ganguly, Nucl. Phys. **A101**, 589 (1967).

³³J. Dudek, W. Nazarewicz, and T. Werner, Nucl. Phys. **A341**, 253 (1980).

³⁴J. S. Hanspal, Ph.D. Thesis, University of London, 1982 (unpublished).

³⁵C. J. Batty and G. W. Greenlees, Nucl. Phys. **A133**, 673 (1969); C. J. Batty, Phys. Lett. **31B**, 496 (1970).

³⁶S. A. A. Zaidi and S. Darmodjo, Phys. Rev. Lett. **19**, 1446 (1967).

³⁷B. A. Brown, S. E. Massen, and P. E. Hodgson, J. Phys. G **5**, 1655 (1979).

³⁸B. A. Brown (private communication).

³⁹G. J. Pyle, University of Minnesota Report No. COO-1265-65, 1965.

⁴⁰P. M. Lewis (private communication); P. M. Lewis, O. Karban, A. K. Basak, E. C. Pollacco, and S. Roman, in *Polarization Phenomena in Nuclear Physics—1980 (Fifth International Symposium, Santa Fe)*, Proceedings of the Fifth International Symposium on Polarization Phenomena in Nuclear Physics, AIP Conf. Proc. No. 69, edited by G. G. Ohlson, R. E. Brown, N. Jarmie, M. W. McNaughton, and G. M. Hale (AIP, New York, 1981), p. 590.

⁴¹F. Entezami, A. J. Basak, O. Karban, P. M. Lewis, and S. Roman, Nucl. Phys. **A366**, 1 (1981).

⁴²H. J. Trost *et al.*, Nucl. Phys. **A337**, 377 (1980).

⁴³G. Bertsch and R. Schaeffer, J. Phys. (Paris) **40**, 1 (1979).

⁴⁴W. J. Thompson, Phys. Lett. **85B**, 180 (1979).